

State-space formulation of scalar Preisach hysteresis model for rapid computation in time domain

Michael Ruderman

Nagaoka University of Technology, Department of Electrical Engineering, Nagaoka, 940-2188, Japan

Abstract

A state-space formulation of classical scalar Preisach model (CSPM) of hysteresis is proposed. The introduced state dynamics and memory interface allow to use the state equation, which is rapid in calculation, instead of the original Preisach equation. The main benefit of the proposed modeling approach is the reduced computational effort which requires only a single integration over the instantaneous line segment in the Preisach plane. Numerical evaluations of the computation time and model accuracy are provided in comparison to the CSPM which is taken as a reference model.

Keywords: Preisach model, scalar hysteresis map, nonlinear state dynamics, hysteresis behavior

1. Introduction

The Preisach-based modeling approaches [1]–[4] are widely used to describe the hysteresis effects of different nature. The classical scalar Preisach model (CSPM) bases upon two mathematical properties: wiping-out and congruency [2]. Numerous extensions of CSPM [4] were proposed over the last decades in order to overcome several discrepancies between CSPM and hysteresis effects experimentally observable in magnetic materials and structures. Among these are the non-congruency of minor hysteresis loops, rate-dependency (or dynamic generalization) of hysteresis, as well as stabilization process (or accommodation) which violates the wiping-out hysteresis property. The evolution of Preisach-type hysteresis models has been illustrated e.g. in [5]. Further reformulations of CSPM such as DOK model [6] and so-called modified scalar Preisach model (MSPM) [7] were proposed for a fast hysteresis computation and with regard to reversible components of magnetization. A comparative study of DOK and MSPM scalar hysteresis models is also given in [8]. Despite a continuous advancement in hysteresis modeling the CSPM remains a still significant means for simulation and control tasks shown in various applications, see e.g. [9], [10], [11]. It is worth noting that also another than Preisach formalisms, e.g. Duhem [12] or first-order nonlinear differential equations [13], [3] have been widely used for modeling hysteresis. For instance the dissipativity property and stability of systems with the Duhem hysteresis operator have been recently studied in [14]. Further, the so-called butterfly-shaped hysteresis map and its conversion to simple piecewise monotone hysteresis maps has been analyzed in [15]. The significance of appropriate hysteresis modeling in control can be seen for both cases: immediate use as an inverse filter for compensating hysteresis [16], and analyzing the effect of hysteresis on the stability of control system to be designed.

When using a Preisach-type hysteresis modeling, in particular the computational efficiency is required due to a large number of hysteresis operators, which are spatially distributed in space of the threshold values. Especially, a continuous (dynamic) hysteresis behavior is computationally intensive since the smooth input time series provoke continuous changes of the hysteresis output. Here it should be noted that the smooth input time series relate to the physical signals in various applications where the input jumps and impact of noise are excluded from consideration, e.g. simulation and/or feed-forwarding of controlled processes.

Email address: ruderman@vos.nagaokaut.ac.jp (Michael Ruderman)

The purpose of this communication is to provide a state-space formulation of CSPM in order to reduce the original computation costs without losing significantly the model accuracy at certain sampling conditions. The proposed modeling approach was first shown at the International Symposium on Hysteresis and Micromagnetics Modeling (HMM2011) and since then applied in the discrete-time form in [17, 18]. In the recent work, the general continuous-time and continuous-state case is provided in details. The main benefit is the computation effort reduced from the double integration over the Preisach plane to a single integration over the line segment at an operation state. In Landau notation it means that the computation complexity of CSPM, which is originally $\mathcal{O}(n^2 + 1)$, is reduced to $\mathcal{O}(n + 1)$. Here, it is important to note that the majority of Preisach-type hysteresis modeling approaches use the so called first-order reversal curves (FORC), see e.g. [2], [4] for details, so as to avoid the double integration. This widely elaborated and well-implementable approach provides indeed a fast hysteresis computation, but, at the same time, requires discretizing the Preisach plane in order to store a finite set of FORCs. This does not allow applying the continuous and parametric Preisach distribution functions and limits the simulation capabilities to the discretized input-output maps. In rest of the paper the details of the proposed model formulation and various numerical evaluation examples are given.

2. State-space formulation

In order to provide the CSPM in state-space formulation let us briefly summarize first the main CSPM equations and geometrical interpretation by means of the Preisach plane (further denoted by P). The basic input-output map of Preisach hysteresis operator $H[\cdot]$ is given by

$$y(t) = H[x(t)] = \iint_{\alpha \geq \beta} \rho(\alpha, \beta) h_{\alpha\beta}[x(t)] d\alpha d\beta. \quad (1)$$

The elementary hysteresis operator (*hysteron*) $h_{\alpha\beta}[\cdot]$ constitutes a non-ideal (delayed) relay with 'up' and 'down' threshold values α and β . The main parametrization factor of CSPM is the Preisach density function (PDF) $\rho(\alpha, \beta)$ defined over $P = \{(\alpha, \beta) \mid \alpha \geq \beta\}$. At each instant t the plane P is divided into two disjunct subsets, $P^+(t)$ which contains the hysterons in the 'up' state (+1) and $P^-(t)$ which contains the residual hysterons in the 'down' state (-1). Both subsets are separated by a staircase interface L , as illustrated schematically in Figure 1, which constitutes the instantaneous memory state of hysteresis. According to

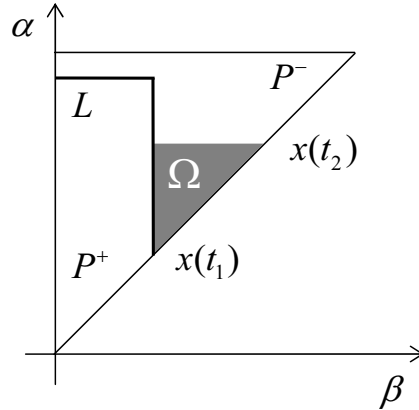


Figure 1: Preisach plane with switching region

$h_{\alpha\beta} : x \mapsto \{-1, +1\}$ and with respect to $P(t) = P^+(t) \cup P^-(t)$ one can easily obtain

$$\begin{aligned} y(t) &= \iint_{P_+} \rho(\alpha, \beta) d\alpha d\beta - \iint_{P_-} \rho(\alpha, \beta) d\alpha d\beta = \\ &= 2 \iint_{P_+} \rho(\alpha, \beta) d\alpha d\beta - \iint_P \rho(\alpha, \beta) d\alpha d\beta. \end{aligned} \quad (2)$$

When increasing the input, starting from $x(t_1)$ and going monotonically to $x(t_2)$ with $t_2 > t_1$, the hysterons within the switching region Ω transit to the 'up' state, thus changing from P^- to P^+ . The output difference $\Delta y = y(t_2) - y(t_1)$ can be obtained from Eq. (2) as

$$\begin{aligned}\Delta y &= \int_{P^+(t_2)} \rho(\alpha, \beta) d\alpha d\beta - \int_{P^+(t_1)} \rho(\alpha, \beta) d\alpha d\beta = \\ &= \int_{\Omega} \rho(\alpha, \beta) d\alpha d\beta ,\end{aligned}\tag{3}$$

this with respect to the set definition $P^+(t_2) = P^+(t_1) \cup \Omega$. Since the Preisach hysteresis function is monotonic and the variable switching region captures the output difference for all increasing and decreasing branches one can write the general form of the output difference as

$$\Delta y = 2 \operatorname{sgn}(\Delta x) \int \int_{\Omega(\Delta x)} \rho(\alpha, \beta) d\alpha d\beta .\tag{4}$$

Equation (4) is valid for all input differences $\Delta x = x_2 - x_1$ at finite time $\Delta t = t_2 - t_1 > 0$. Note that CSPM constitutes a rate-independent hysteresis map so that Δy depends on Δx only and not on Δt .

Now consider the continuous nonlinear model

$$\frac{d\mathbf{z}}{dt} = \mathbf{f}\left(\mathbf{z}, \frac{dx}{dt}\right)\tag{5}$$

with the state vector \mathbf{z} which contains the output value $y(t)$ and memory vector $\mathbf{m}(t) = m \cup M$. The latter is an ordered set of alternating local minima

$$m \subset \{x(t) \mid \dot{x}(t) = 0 \wedge x(t_+) > x(t) \wedge t_0 < t < t_+\}\tag{6}$$

and maxima

$$M \subset \{x(t) \mid \dot{x}(t) = 0 \wedge x(t_+) < x(t) \wedge t_0 < t < t_+\} .\tag{7}$$

Recall that only the local extrema, which fulfill the wiping-out hysteresis property [2], are stored in the memory vector and constitute the (α, β) vertexes of the interface L between P^+ and P^- . That is each novel m item, according to Eq. (6), is not only included to $\mathbf{m}(t)$ but also erases from $\mathbf{m}(t)$ all the previously stored minima which are less than the recent one. The same mechanism is acting for each novel M item which is larger than the previously stored local maxima. Since the ground state (or ‘‘demagnetized state’’ in context of magnetism [2]) of hysteresis is determined by the main diagonal $\alpha = -\beta$ (in the Preisach plane) the initial states (at $t = 0$) are

$$y_0 = 0 \quad \text{and} \quad \mathbf{m}_0 = \begin{bmatrix} x_{max} & x_{min} \\ 0 & 0 \end{bmatrix} .\tag{8}$$

Note that the (x_{max}, x_{min}) vertex, which is the opposite end of L relating to the operation point $(x(t), x(t))$, is required to margin the Preisach plane in the implementation.

When taking the limiting value $\Delta x \rightarrow 0$ and dividing the left- and right-hand sides of Eq. (4) by the time derivative the output state equation is represented by

$$\frac{dy}{dt} = 2T \operatorname{sgn}(dx) \int \int_{\Omega(dx)} \rho(\alpha, \beta) d\alpha d\beta .\tag{9}$$

Note that the state equation (9) complies with the general one given in Eq. (5), since Ω is obtained using the instantaneous memory state and dx value. The latter is available for a constant computation rate, i.e. $dt = \text{const} = 1/T$.

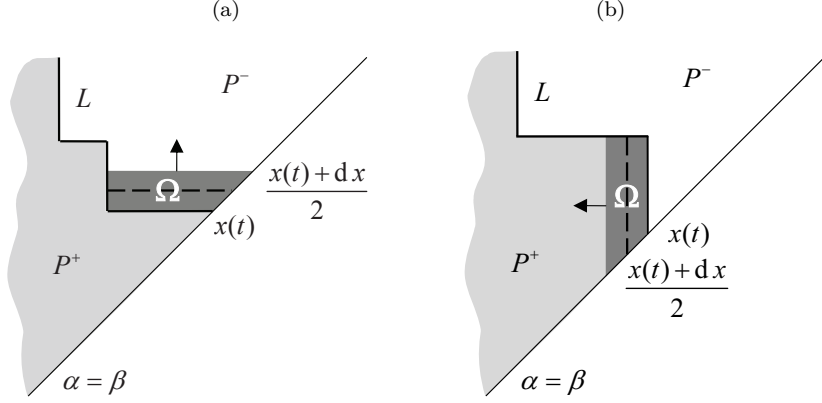


Figure 2: Integral area by increasing (a) and decreasing (b) input

In order to integrate PDF over the variable switching region consider an arbitrary hysteresis state, once for increasing and once for decreasing input as exemplarily shown in Figure 2. Since $\Delta x \rightarrow 0$ the switching region converges to a line segment with $\alpha = (x(t) + dx)/2$ for increasing, and $\beta = (x(t) + dx)/2$ for decreasing input value. Hence, the opposite end of the line segment is determined by the latest stored minima (m_l) for $dx > 0$ and maxima (M_l) for $dx < 0$ correspondingly. Hence, the double integration over the switching region can be replaced by the single integration over the line segment when $|dx|$ is small enough. Denoting the $(x(t) + dx)/2$ value by $x_+ \forall dx > 0$ and by $x_- \forall dx < 0$ the state equation of hysteresis output can be rewritten as

$$f_1 = \begin{cases} 2T \operatorname{sgn}(dx) \int_{\beta(m_l)}^{x_+} \rho(x_+, \beta) d\beta, & \text{if } dx > 0 \\ 2T \operatorname{sgn}(dx) \int_{\alpha(M_l)}^{x_-} \rho(\alpha, x_-) d\alpha, & \text{if } dx < 0 \\ 0, & \text{otherwise.} \end{cases} \quad (10)$$

Since the hysteresis memory state is described by a set of (α, β) vertexes the memory state equation $d\mathbf{m}/dt = f_2(\mathbf{z}, dx/dt)$ should be introduced by means of a dedicated operator

$$f_2 = \begin{cases} O_1^+ \wedge O_2^+ \wedge O_3^+, & \text{if } dx > 0 \\ O_1^- \wedge O_2^- \wedge O_3^-, & \text{if } dx < 0 \\ \emptyset & \text{otherwise,} \end{cases} \quad (11)$$

using the algebra of sets. Note that the operator f_2 is not commutative concerning O_i , because of the ordered set of the memory vector. The single set operators

$$O_{1,\dots,3}^+ = \begin{cases} \setminus \{m, M \mid \alpha \leq x_+\} \\ \cup (x_+, \beta(M_l)) \\ \cup (x_+, x_+) \end{cases} \quad (12)$$

and

$$O_{1,\dots,3}^- = \begin{cases} \setminus \{m, M \mid \beta \geq x_-\} \\ \cup (\alpha(m_l), x_-) \\ \cup (x_-, x_-) \end{cases} \quad (13)$$

modify the memory state vector at each instant t , where the last case in Eq. (11) denotes no changes of \mathbf{m} when $dx = 0$. The first case in Eqs. (12) and (13) constitutes the wiping-out hysteresis property, and

the second and third cases correspondingly update the last local extremum and insert the actual operation point.

The introduced state equations capture the entire hysteresis behavior independent of the initial state $[y_0, \mathbf{m}_0]$ which is assumed to be known. Note that when computing the output value

$$y(t) = 2T \int_0^t \text{sgn}(dx(t)) \iint_{\Omega(dx(t))} \rho(\alpha, \beta) d\alpha d\beta dt \quad (14)$$

the state equation (11) has to be evaluated first before integrating the output dynamics.

3. Numerical evaluation

The proposed scalar Preisach model in a state-space formulation (further as SSPM) is implemented in a dedicated software code working within MATLAB[®] computation environment. All simulation results below are obtained on an ordinary PC powered by an Intel Duo CPU, 2 GHz, with 4 GB random access memory (RAM). The numerical integration is performed using the standard routine with adaptive Lobatto quadrature, where the set error tolerance (*tol*) constitutes the main parametrization factor which impacts both the integration accuracy and computation time.

Three different parametric PDFs and that the uninform distribution (abbreviated by U), biased exponential distribution (abbreviated by E), and Gaussian mixture of three weighted normal distributions (abbreviated by G), are taken for the model evaluation. The U-PDF of level v is given by

$$\rho^U(\alpha, \beta) = v.$$

The E-PDF with free parameters A , B , and C is captured by

$$\rho^E(\alpha, \beta) = A \exp(-B|(\alpha, \beta)|) + C.$$

The G-PDF with Gaussian components $\mathcal{N}(\mu, \Sigma)$, each one parameterized by the mean vector μ and symmetric covariance matrix Σ (both in the (α, β) coordinates) and weighted by w , is given by

$$\rho^G(\alpha, \beta) = \sum_{i=1}^3 w_i \mathcal{N}(\mu_i, \Sigma_i)[\alpha, \beta].$$

The assumed (α, β) distributions and the corresponding major hysteresis loops started from the ground state are depicted in Figure 3. Note that the number of parameters of U-, E-, and G-PDFs accounts for 1, 3, and 18 correspondingly.

3.1. Comparison of CSPM and SSPM

First, the computation time and accuracy of SSPM are compared with those achieved by CSPM as it is provided in Eq. (1). Three error tolerance values (*tol*), $1e^{-3}$, $1e^{-4}$, and $1e^{-5}$ set for numerical integration are taken into evaluation. The maximal $\hat{\tau}$ and average $\bar{\tau}$ computation time required to determine one closed (major) hysteresis loop, as well as its standard deviation $\tilde{\tau}$, are taken as performance metrics (*pm*) of the computation effort. In order to evaluate the model accuracy the CSPM response with $1e^{-5}$ *tol* value is taken as reference (*ref*) since that one provides a most exact, but also most time-consuming, integration of PDF. The accuracy performance metrics – maximal \hat{e} and average \bar{e} error as well as the error standard deviation \tilde{e} – rely on the relative error normalized by the overall hysteresis magnitude as

$$e(x(t)) = \frac{|y(t) - y_{ref}(t)|}{|y_{max} - y_{min}|} \times 100\%. \quad (15)$$

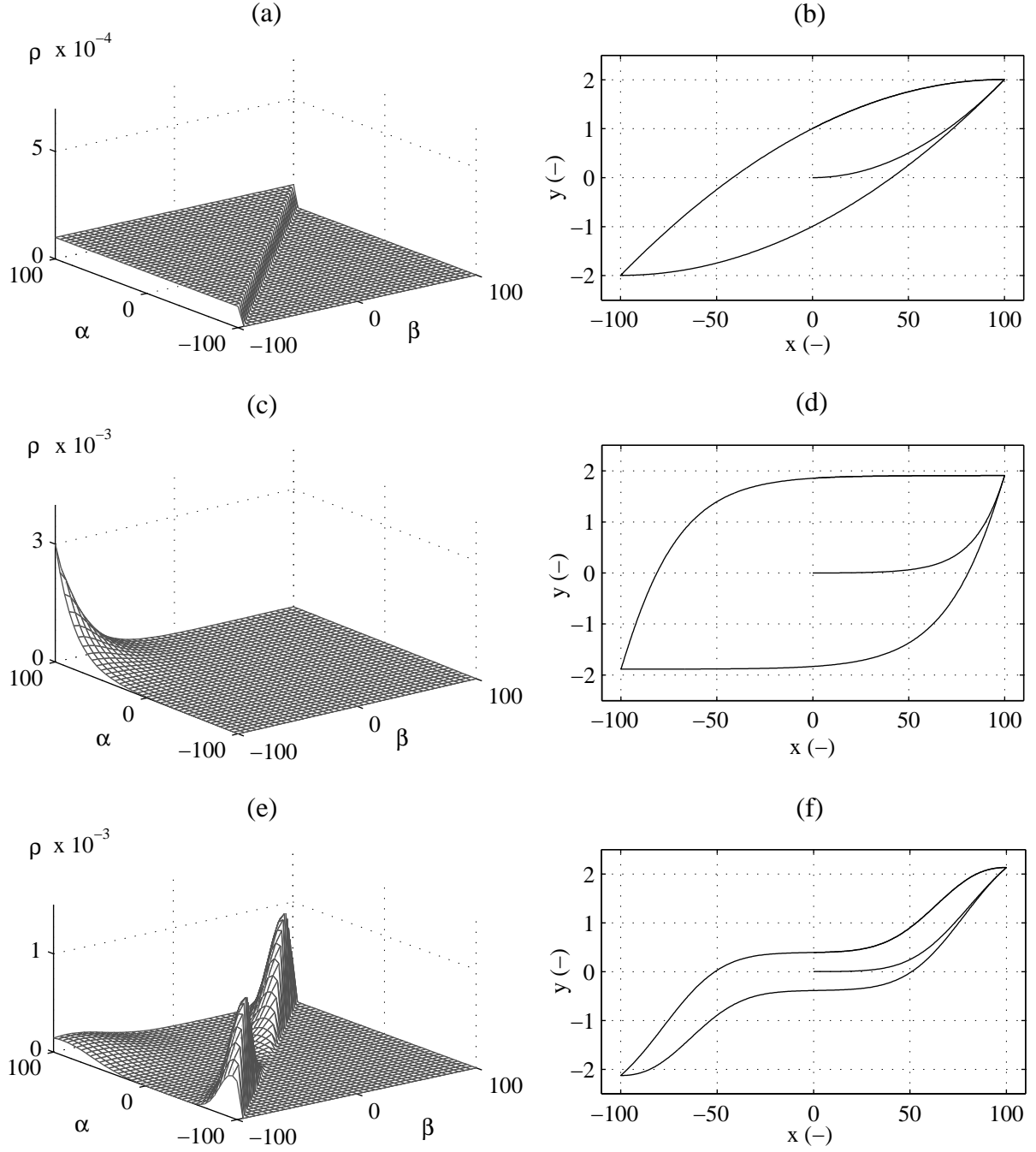


Figure 3: Parametric PDFs and corresponding hysteresis loops: uniform (a-b); Gaussian mixture (c-d); biased exponential (e-f)

One closed (major) hysteresis loop is computed using the periodic input $x(t) = 100 \sin(2\pi t - \pi/2)$ and having the simulation sampling time 0.001 sec. Thus, 1000 time-equidistant (x, y) data tuples per hysteresis loop are recorded for evaluation. The defined performance metrics of computation time and accuracy are compared in Table 1 for CSPM and SSPM. Note that the computation time metrics are denoted in milliseconds (ms), and accuracy metrics are denoted in percent (%).

Table 1: Computation time and accuracy metrics of CSPM and SSPM

case			U-PDF		E-PDF		G-PDF	
<i>tol</i>	<i>pm</i>	unit	CSPM	SSPM	CSPM	SSPM	CSPM	SSPM
$1e^{-3}$	$\hat{\tau}$	ms	100	0.70	18.3	1.70	195	9.30
	$\bar{\tau}$	ms	49.9	0.33	9.30	0.35	48.1	4.20
	$\tilde{\tau}$	ms	36.7	0.26	4.80	0.14	48.2	2.30
	\hat{e}	%	1.22	2.80	0.57	0.22	4.89	2.15
	\bar{e}	%	0.32	1.62	0.23	0.18	2.00	1.09
	\tilde{e}	%	0.38	0.90	0.24	0.18	2.25	1.15
$1e^{-4}$	$\hat{\tau}$	ms	349	1.30	58.8	2.40	3600	14.2
	$\bar{\tau}$	ms	165	0.72	13.5	0.45	499	7.30
	$\tilde{\tau}$	ms	129	0.32	10.6	0.25	588	3.40
	\hat{e}	%	0.34	0.58	0.21	0.12	0.96	0.58
	\bar{e}	%	0.17	0.40	0.03	0.05	0.19	0.33
	\tilde{e}	%	0.19	0.13	0.04	0.04	0.24	0.13
$1e^{-5}$	$\hat{\tau}$	ms	495	3.00	172	2.30	4446	20.2
	$\bar{\tau}$	ms	210	1.30	39.0	0.55	721	12.6
	$\tilde{\tau}$	ms	164	0.48	27.7	0.39	791	3.70
	\hat{e}	%	ref	0.03	ref	0.12	ref	0.06
	\bar{e}	%	ref	0.01	ref	0.05	ref	0.02
	\tilde{e}	%	ref	0.01	ref	0.04	ref	0.02

It is evident that the *tol* value $1e^{-5}$ provides the most accurate but also the slowest hysteresis computation, and that for all considered PDFs. Here, the accuracy metrics of SSPM fall under 0.1 % which is reasonably an acceptable value, particularly in regard to unavoidable data errors when identifying the hysteresis. The computation time metrics of SSPM are cardinally superior in comparison to CSPM. Almost all τ -metrics of SSPM are 100–200 times lower than these of CSPM, excepting the E-PDF case with lower *tol* values at which the differences are about 10–20 times. Remarkable is the fact that a decrease of *tol* value from $1e^{-3}$ to $1e^{-5}$, i.e. of two orders, leads to an increase of τ -metrics in the range of 5–20 times for CSPM, where the τ -metrics of SSPM increase in the range of 1.5–3 times only.

3.2. Integration accuracy of SSPM

Since the computation of SSPM output bases on a continuous integration of dynamic state, the integration errors of a cumulative character can significantly disturb the model accuracy. Besides an inherent accuracy, determined by the set error tolerance value, the chosen finite sampling time dt can additionally influence the state values computed according to Eq. (9), while the equal input sequence is applied. It is evident that a lower sampling time leads to a higher model accuracy since this reduces dx , thus capturing the switching region by the corresponding line segment in a more accurate way. Two different multi-sinus input sequences with a bandwidth 0.1–10 Hz are evaluated on SSPM for the assumed U-PDF. The first one is symmetrical to zero and the second one is biased, so that the hysteresis operates predominantly in the first quadrant. The resulting hysteresis response is visualized in Figure 4 (a) and (b) correspondingly.

In order to evaluate the integration accuracy of SSPM the sampling rate of 10 kHz is taken as the reference. The reduced sampling rates of 5 kHz and 1 kHz are evaluated in terms of the output divergence comparing to the output obtained at 10 kHz. In Figure 5 the hysteresis output and the evaluated relative error are depicted for both multi-sinus sequences. It is evident that the error obtained at 5 kHz sampling rate is lower than that obtained at 1 kHz. Particularly, the fast higher peaks of hysteresis input, and consequently output, lead to a higher relative error. It comes as not surprising since the higher input harmonics result in an increase of dx , while dt remains constant. Another important aspect is a slight drift of the relative error

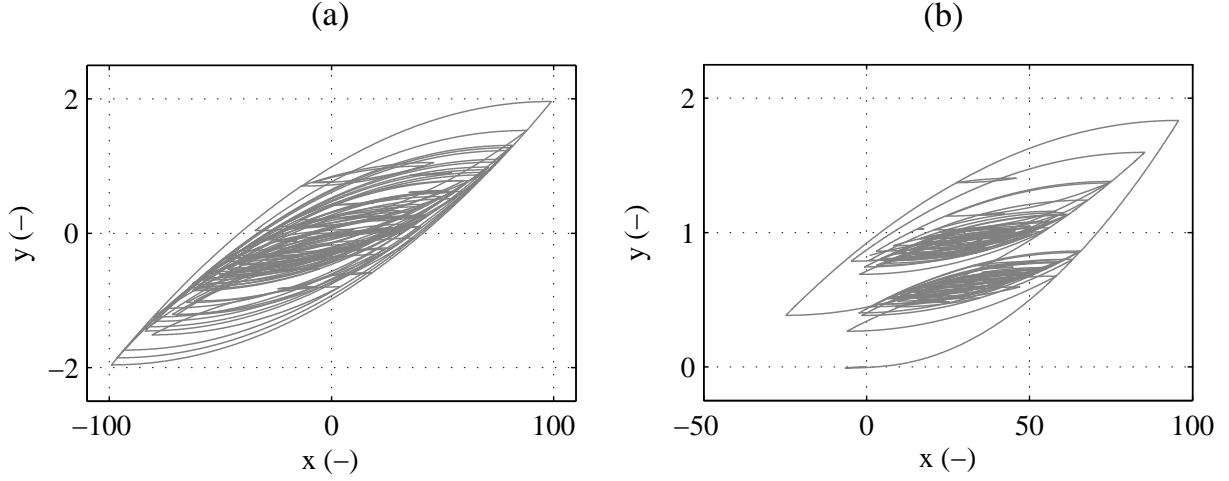


Figure 4: Hysteresis response to the multi-sinus (0.1–10 Hz) input sequence: (a) zero symmetrical, (b) zero biased

observable in case of the biased multi-sinus input. This appears since the DC signal component provokes an integrating output error. However, the latter can remain alternating around the DC bias when the total number of ascending and descending hysteresis branches are well balanced. A more extensive analysis of integration error dynamics and evaluation of different numerical solver types could help characterizing better the model accuracy in the future works.

4. Conclusions

In this paper, a state-space formulation of scalar Preisach hysteresis model has been introduced. By doing this the main Preisach formalism and model properties, i.e. wiping-out and congruency, are not violated. Using the same geometrical interpretation by means of the Preisach plane and hysteresis density function, which is the principal parametrization factor, the dynamic state variables of hysteresis memory and output have been introduced.

When using the Preisach hysteresis model in its original formulation, the double integration of Preisach density function over the operation space of hysterons is required. In this work, the original computation cost have been reduced without losing significantly the model accuracy. In Landau notation, the computation complexity has been reduced from $\mathcal{O}(n^2 + 1)$ to $\mathcal{O}(n + 1)$, since the double integration over the Preisach plane was replaced by the single integration over the line segment determined by the operation state. Multiple numerical evaluating tests have shown that the computation time performance can be increased up to 100 times in comparison to the classical scalar Preisach model. We note that the integration errors of computing the dynamic state variable are the main sources of model inaccuracies. However, reducing the error tolerance of numerical integration and keeping an appropriate relation between the sampling and input rate a fast and accurate model can be achieved.

Finally it can be concluded that the proposed state-space formulation of classical scalar Preisach model is well suitable for multiple hysteresis applications independent of the physical nature and shape of congruent hysteresis loops. The modeled hysteresis has, however, to comply with the assumed Preisach hysteresis properties (see e.g. in [2]).

References

- [1] F. Preisach, Ueber die magnetische Nachwirkung, Zeitschrift Physik 94 (1935) 277–302.
- [2] I. D. Mayergoyz, Mathematical models of hysteresis and their application, 2nd Edition, Academic Press an imprint of Elsevier, Amsterdam, Netherlands, 2003.

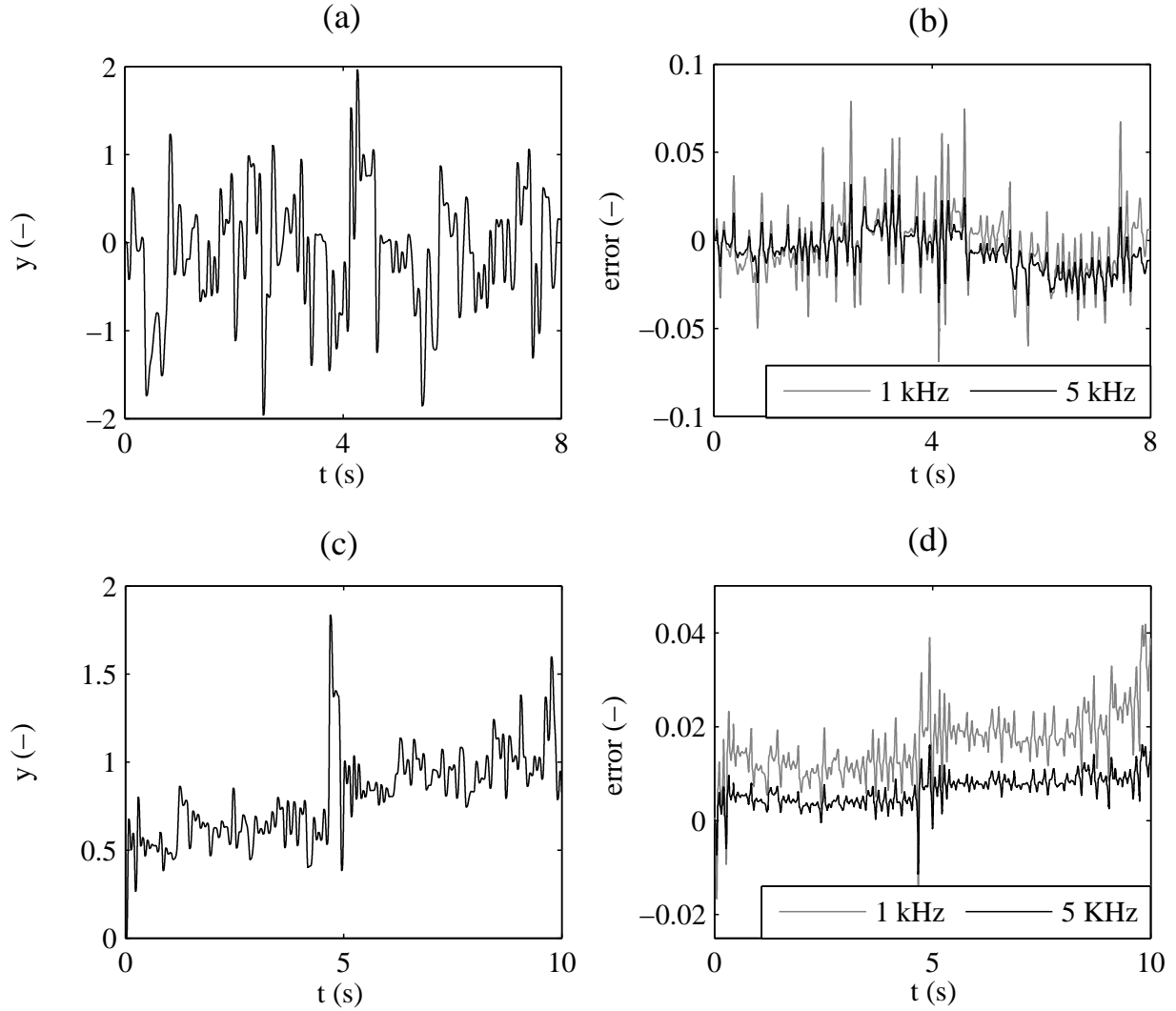


Figure 5: Hysteresis output and evaluated relative error for different sampling rates: (a-b) zero symmetrical, (c-d) zero biased

- [3] A. Visintin, *Differential Models of Hysteresis*, 1st Edition, Springer, Berlin-Heidelberg, Germany, 1994.
- [4] G. Bertotti, I. D. Mayergoyz, *The Science of Hysteresis 1-3*, 1st Edition, Academic Press, 2006.
- [5] O. Bottauscio, M. Chiampi, D. Chiarabaglio, M. Repetto, Preisach-type hysteresis models in magnetic field computation, *Physica B: Condensed Matter* 275 (2000) 34–39.
- [6] E. D. Torre, J. Oti, G. Kadar, Preisach modeling and reversible magnetization, *IEEE Transactions on Magnetics* 26 (6) (1990) 3052–3058.
- [7] E. Cardelli, E. D. Torre, B. Tellini, Direct and inverse preisach modeling of soft materials, *IEEE Transactions on Magnetics* 36 (4) (2000) 1267–1271.
- [8] B. Azzerboni, E. Cardelli, G. Finocchio, A comparative study of preisach scalar hysteresis models, *Physica B: Condensed Matter* 343 (2004) 164–170.
- [9] L. Dupre, R. V. Keer, J. Melkebeek, A computational model for the iron losses in rotating electrical machines, *International Journal of Engineering Science* 36 (7–8) (1998) 699–709.
- [10] C. Natale, F. Velardi, C. Visone, Identification and compensation of preisach hysteresis models for magnetostrictive actuators, *Physica B: Condensed Matter* 306 (2001) 161–165.
- [11] S. Rosenbaum, M. Ruderman, T. Stroehla, T. Bertram, Use of Jiles-Atherton and Preisach Hysteresis models for inverse feed-forward control, *IEEE Transactions on Magnetics* 46 (12) (2010) 3984–3989.
- [12] G. Gentili, C. Giorgi, A new model for rate-independent hysteresis in permanent magnets, *International Journal of Engineering Science* 39 (9) (2001) 1057–1090.

- [13] L. O. Chua, K. A. Stromsmoe, Mathematical model for dynamic hysteresis loops, *International Journal of Engineering Science* 9 (5) (1971) 435–450.
- [14] B. Jayawardhana, R. Ouyang, V. Andrieu, Stability of systems with the duhem hysteresis operator: The dissipativity approach, *Automatica* 48 (10) (2012) 2657–2662.
- [15] B. Drincic, X. Tan, D. S. Bernstein, Why are some hysteresis loops shaped like a butterfly?, *Automatica* 47 (12) (2011) 2658–2664.
- [16] X. Tan, J. S. Baras, Modeling and control of hysteresis in magnetostrictive actuators, *Automatica* 40 (9) (2004) 1469–1480.
- [17] M. Ruderman, T. Bertram, Identification of soft magnetic B-H characteristics using Discrete Dynamic Preisach model and single measured hysteresis loop, *IEEE Transactions on Magnetics* 48 (4) (2012) 1281–1284.
- [18] M. Ruderman, T. Bertram, Control of magnetic shape memory actuators using observer-based inverse hysteresis approach, *IEEE Transactions Control Systems Technology* 22 (3) (2014) 1181–1189.